

Understanding People Flow in Transportation Hubs

João Carvalho, Manuel Marques, João P. Costeira

Abstract—In this paper, we aim to monitor the flow of people in large public infrastructures. We propose an unsupervised methodology to cluster people flow patterns into the most typical and meaningful configurations. By processing 3D images from a network of depth cameras, we built a descriptor for the flow pattern. We define a data-irregularity measure that assesses how well each descriptor fits a data model. This allows us to rank the flow patterns from highly distinctive (outliers) to very common ones and, discarding outliers, obtain more reliable key configurations (classes).

We applied this methodology in an operational scenario during 18 days in the X-ray screening area of an international airport. Results show that our methodology is able to summarize the representative patterns, a relevant information for airport management. Beyond regular flows our method identifies a set of rare events corresponding to uncommon activities (cleaning, special security and circulating staff). We demonstrate that for such a long observation period our methodology encapsulates the relevant “states” of the infrastructure in a very compact way.

Index Terms—People flow monitoring, unsupervised clustering, depth cameras

I. INTRODUCTION

In this article, we address the problem of crowd monitoring in public infrastructures. We propose a sensing and data processing framework which captures crowd occupancy in these large spaces, and identifies and classifies it into meaningful spatial patterns/classes. We tested it in a real-life scenario in the main security X-ray screening area at the Lisbon international airport (LIS), Portugal.

Airports are transportation hubs subject to strict service-level agreements (SLA), high security risks and high operational costs. These factors put great pressure on human and physical resources, calling for tight monitoring of passenger flow within the infrastructure. In particular, the security and identification checkpoints are critical bottlenecks in the path between the check-in and the departure gate. Besides the risk of SLA violation, these bottlenecks have great impact on operational and commercial costs. Our work focuses on characterizing how passengers flow while waiting for inspection in these critical checkpoints.

The sensing infrastructure we propose consists of a network of depth cameras that provide 3D data of the covered space. A set of pre-processing algorithms anonymously detect people in the 3D point cloud, count them and compute the 3D space occupancy map as the output data of the sensing system. Fig. 1 displays the specific geometry of LIS X-ray area¹. All passengers enter from the right, wait for their turn and exit to the left towards individual X-ray booths. In such a large space—more than 200m²—several configurations emerge, shaped by

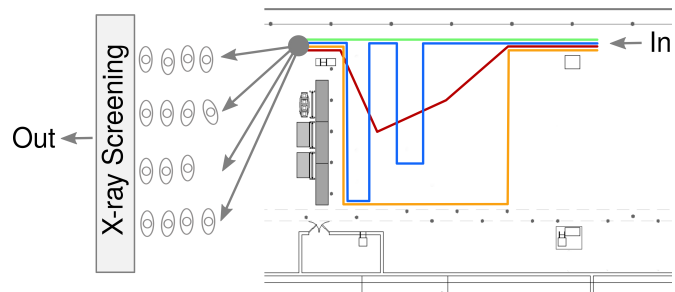


Fig. 1. X-ray screening queue area at the Lisbon international airport. The colored lines illustrate examples of paths in the queue area. The queue area is around 200m².

inflow variations, processing capacity, planning protocols and particular events.

Currently, the global status of the X-ray system is monitored using global counts of in-out passenger flow [1], [2]. These global measures do not account for the internal state of the queue that reflects the instantaneous operating condition of the whole system. Queue modeling (e.g. flow parametrization) is very difficult to do, despite some structure imposed by queue guides and a relatively controlled environment. X-ray queue configurations are set in an ad-hoc manner and often change according to discretionary decisions by operations personnel. Also, innumerable “small” local decisions impact the global system: metal detectors settings, protocols for suspicious luggage screening, passenger inspection or security personnel skills. All these aspects are hard to account for but affect the performance and overall state of the X-ray queue.

Our methodology for classification of passenger flow patterns identifies meaningful classes that encode space occupancy. Classes are defined by space occupancy patterns that appear regularly over time (*regular* patterns) as well as sporadic patterns that correspond to “atypical behaviours” (*irregular* patterns). Because of the large amount of data, it is very difficult for the airport management to define the most relevant classes.

Building on previous work in the computer vision domain [3], we encode regularity/irregularity through linear subspace models that explicitly represent these regularity concepts [4], [5]. Such subspaces are determined from data in an unsupervised way.

Our methodology grants decision-makers with the much sought holistic measure of the “operational state” of the infrastructure. The methodology is general and applicable to a wide variety of public infrastructures such as railway stations or commercial shopping centers.

In summary, our main contributions are:

- a 3D sensing infrastructure for queue data collection;

The authors are with the Institute for Systems and Robotics (ISR/IST), Instituto Superior Técnico, Universidade de Lisboa, Portugal.

¹The physical infrastructure described here no longer exists.

- a descriptor computed from 3D data of multiple cameras that captures queue patterns;
- an algorithm that explicitly models and identifies *regular* and *irregular* flow patterns and clusters the regular data into classes of “typical” operation modes.

By identifying regular “operating states” of the whole system, airport experts are able to rank and map them to desirable performance indicators. This interaction with the management and operational staff is very important in order to understand the behavior of the whole system [6]. Our methodology can be understood as a pre-processing stage whose information can feed the planning, scheduling and performance analysis systems of the airport.

A. Outline of the paper

The paper is structured as follows. Section II presents the related work, followed by the sensing infrastructure and the queue descriptor in Section III. Section IV provides the setup validation. Section V describes our methodology for identifying regular periods and clustering the data into an unknown number of queue states. The implementation results are presented in Section VI, followed by discussion in Section VII, and the conclusions in Section VIII.

II. PREVIOUS WORK

In complex environments such as an airport [7], the flow of passengers depends on a large number of variables: staff performance, passenger behaviour, hand luggage contents, sensitivity of metal detection systems, among others. Traditional approaches based on discrete event systems [8], [9] or queueing theory [10]–[12] model airport activity as function of several such variables. However, these methods are difficult to tune because they are highly dependent on variables that are unobservable or modeled with (unrealistic) stationary distributions (*e.g.*, arrival and service rates). Also, these are based on data manually acquired within limited time frames or based on aggregated statistics. Besides providing tools for real time data acquisition, our methodology identifies the stationary states of the queue, allowing the design of individual and more accurate models for each state.

To automatically acquire people flow data, several works track and count people with a single over-the-head RGB-D camera [13]–[15]. Similar approach was taken in [16], [17] for a single video camera.

In crowded scenes, instead of tracking people individually, several works propose solutions for activity detection or estimation of the number of people present in the scene. For example, Convolutional Neural Networks (CNN) are employed in [18] to compute a per-pixel crowd counting map in order to estimate the number of people crossing a line. [19] improves crowd counting by training a CNN using two related objectives, crowd density and count, to obtain a better local optimum for both. Alternatively, [20] proposes a multi-column CNN to map an image to its crowd density map. In [21] and [22], the authors use features derived from optical flow to train a system for counting people in regions of interest at crowded places. The first analyzes the optical flow passing through a

line orthogonal to the motion of people and the latter tracks the boundary of a region of interest. The optical acceleration and histogram of optical flow gradients can be combined to detect abnormal objects or speed violation in pedestrian scenes [23]. A probabilistic approach is employed by Wang *et al.*, [24], to cluster moving pixels and video segments in order to model atomic activities and interactions in crowded places. In [25], the detection of abnormal behaviors is done with a spatio-temporal analysis of a densely sampled video volumes.

Clustering individual trajectories is another common approach to analyze the flow of people. In [26], feature point tracks are clustered and dominant trajectories are identified by fitting polynomials to cluster mean points. Approach [27] proposes the Robust K-means algorithm for clustering data that is less sensitive to the initialization of the K clusters. K-means and agglomerative clustering are used in [28] to cluster trajectories into common patterns. Alternatively, in [29], trajectories are clustered with Fuzzy C-means and modeled with HMM, for trajectory analysis. Also, local distance and similarity measures are frequently employed to cluster and analyze trajectories and flow data [30], [31].

In [32], the authors propose a system for monitoring queues by tracking people using a network of over-the-head video cameras. A solution to integrate existing monitoring technology is proposed in [1]. It studies methodologies for people counting and individual tracking for queue monitoring and behavior analysis.

In our scenario, the placement of the sensors is limited by the infrastructure, leading to large scene perspective distortion, people occlusion and rendering the registration of video cameras unfeasible. Moreover, due to privacy concerns, the use of video cameras is not permitted in many locations, including the security checkpoint at Lisbon Airport. This precludes the use of the referenced approaches, which, besides using RGB cameras, assume: high ceilings, proposing over-the-head solutions [13], [14], [32]; access to airport sensing infrastructure [1]; existence of reliable individual trajectories [26], [28], [29], [33]; absence of outliers in the data, as irregular patterns [27]; and large amounts of training data [18]–[20].

To the best of our knowledge, there is no work proposed for unsupervised identification and classification of people flow patterns from depth data. Our approach is applicable in a large range of scenarios because it does not require a tracking scheme. Also, we bring the novelty of testing our methodology with 18 days of real data acquired at an international airport.

III. SENSING INFRASTRUCTURE AND DATA DESCRIPTOR

In this section, we present the sensing system and the queue pattern descriptor, based on 3D data processing.

Fig. 2 depicts the network of depth cameras installed to cover the final stage of the queue area. Cameras are calibrated and 3D point clouds are registered into a global reference frame. So, from depth images provided by the seven cameras (Fig. 3a), we build a global 3D representation of the space (Fig. 3b). Since we have a noisy sensor and multiple objects in the foreground, we used a procedure we developed [34] to detect people in 3D point clouds (Section III-A).

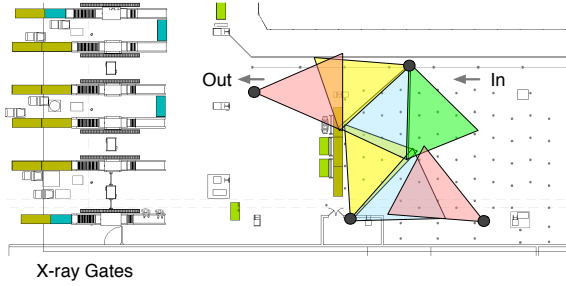


Fig. 2. Camera setup in the X-ray queue with corresponding field of view (FOV). Each colored triangle represents the FOV of a different camera. Passengers enter from the right and exit on the left.

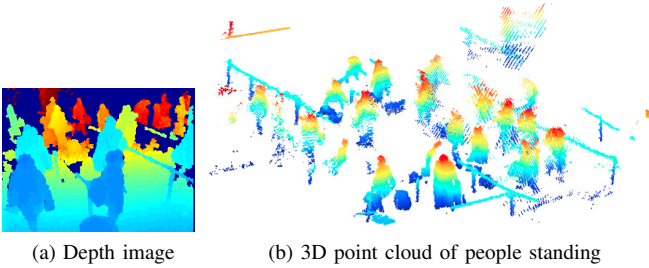


Fig. 3. Depth image and 3D representation: (a) Depth image from one of the cameras placed at the X-ray queue area at the Lisbon International Airport. The value of each pixel represents the depth of the object rather than its brightness or color. The colors are indexed to the distance to the camera, from blue (closer) to dark red (further). Dark blue represents areas not visible by the camera. (b) 3D representation of the space. Colors range from dark blue, for points closer to the ground plane, to dark red, for points further from the ground plane.

Using the results of this detection procedure, we compute a ground occupancy map and use it as a descriptor for the passenger flow (Section III-B).

A. People Detection

The method takes a 3D point cloud as input (Fig. 3b) and outputs the 3D points and centroids corresponding to each person. Fig. 4a shows the 3D point clouds classified as person, with one color per person, and Fig. 4b shows the centroid of each person projected on the ground plane.

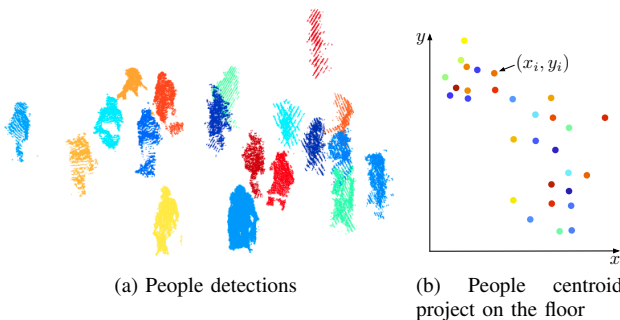


Fig. 4. People detection method results: (a) point cloud of the people detection, with one color per person; (b) centroids (x_i, y_i) of each detection.

The 3D space is scanned with a fixed size box and the point cloud falling within that volume is classified as *person* or *not person*. The classifier, based on random trees, was trained

with point clouds from people in different poses relative to the camera. The output of this method is the labeling of the point cloud and the corresponding centroids in ground coordinates, (x_i, y_i) for person i , as shown in Fig. 4. For details, see [34].

The centroids are used to build the descriptor, as described next.

B. Queue Pattern Descriptor

We propose an occupancy map as data descriptor for the queue state. The floor is discretized into a fixed size grid and we obtain a binary map where each element is set to 1 if occupied and 0 otherwise. A cell is occupied if a centroid falls into it. Fig. 5a shows a set of binary maps, from frame $f - n$ to f .

The occupancy map of a given time period is the spatio-temporal average of the binary maps for the last N seconds². Fig. 5b shows an example of an occupancy map. This map is a vector in \mathbb{R}^d that evolves in time, depending on the space usage, where d is the number of spatial cells of the map.

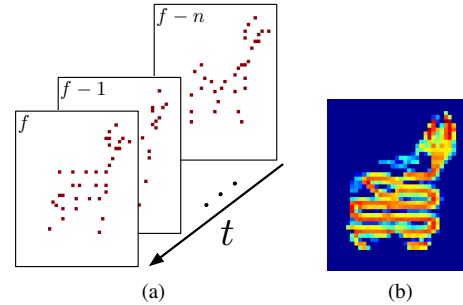


Fig. 5. Occupancy maps: (a) buffer of binary maps; (b) occupancy map for 5min sized buffer. The colors range from dark blue, for the null value, to dark red, for the maximum value of the map.

IV. QUEUE PATTERN VERSUS THROUGHPUT

Based on the people detection procedure, we are able to count people passing in small area at the exit of the queue (Fig. 6). In this scenario, we have 4% error, similar to the classification error obtained on the original paper [34]. Fig.

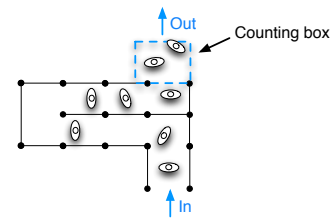


Fig. 6. Illustration of a counting box at the exit of a queue.

7 shows the number of passengers at the entrance (blue line) and at the exit (red line) of the queue during one day. The count at the entrance is provided by the boarding pass scanning system. At the queue exit, our system counts people without distinction between passengers and staff. Therefore,

²A map can be instantaneous or integrated into longer periods, such as 30s, 1min, 5min, 1h.

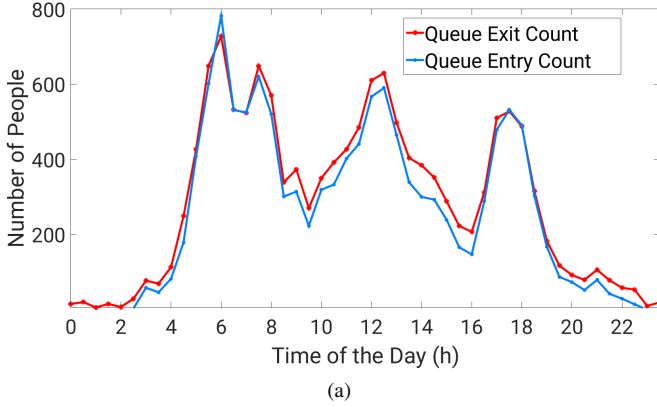


Fig. 7. Number of people passing by the X-ray queue detected with our approach versus ticket validation count. Differences between the two are due to the ground truth being based in boarding pass validation at the entrance of the queue and the count being relative to all the people, including staff, at the exit of the queue. Our detection methodology is able to capture the outflow variation.

the difference between the two counts is due to the detection error, staff passing the queue exit and the delay between the two counting systems, as one is at the entrance and the other at the exit. Despite these sources of error, we can see in Fig. 7 that our detection procedure successfully captures the outflow of the queue. However, the count of passengers is not sufficient to identify the queue state.

Fig. 8 shows four occupancy maps corresponding to four time instants. The periods around 07:00am and 12:00pm

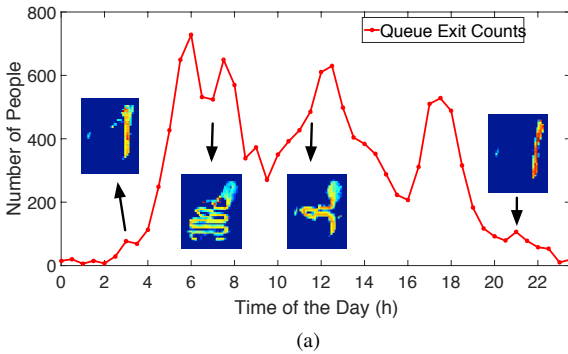


Fig. 8. X-ray exit count versus occupancy maps. Similar counts may correspond to different queue configurations.

have a similar count, however, the queue configurations are different. The state of the queue is dependent on many factors, including, for example, the relation between the queue inflow, service performance and the number of X-ray operating gates. Since these indicators are not available, the outflow of the queue is not enough to determine the queue/service state and we rely on the occupancy map to capture the usage of the space.

V. QUEUE CONFIGURATIONS

In the previous sections, we described our sensing setup composed by a network of depth cameras that provides 3D data. With this data, we are able to detect people and compute

an occupancy grid map – a descriptor that does not rely on tracking to encode people movements.

With the occupancy maps for a given period of time, we aim to cluster them into representative classes, where each class corresponds to a different queue configuration. Fig. 9 illustrates this goal, with similar patterns grouped in the same cluster. Each cluster is represented in different color and with label l_i , where i is the class index. In this example, we illustrate three clusters with regular patterns (l_1 to l_3) and a white label (l_0) for irregular patterns. Since we do not know

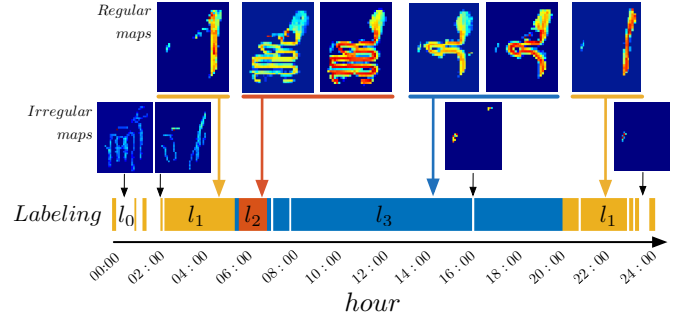


Fig. 9. This figure illustrates the goal of our methodology: going from occupancy maps to labels corresponding to the different queue configurations. Here, we illustrate three regular clusters (l_1 to l_3) and a cluster with irregular patterns (l_0 , white label). Each cluster is composed by several similar patterns.

the classes *a priori*, a supervised approach is not adequate. On the other hand, the traditional unsupervised clustering methods do not guarantee a solution to our problem, as they require the number of classes to be known *a priori* and do not deal with observations without class (outliers). As Fig. 9 shows, we may have a considerable percentage of outliers in the data (white label, l_0).

We model a typical pattern as a linear combination of other maps in the same class and compute the combination coefficients by solving a convex optimization problem. Because typical patterns appear regularly over time, we draw inspiration from the *self-expressiveness* property [4], [5], which states that a point in a subspace can be represented as a linear combination of points in the same subspace. So, each class is modeled as a subspace, where each pattern of a given class is a point in the corresponding subspace. Solving this convex optimization problem, we have a measure of irregularity that assesses how distant a pattern is from the linear model. If this measurement is too high, the pattern is considered irregular (outlier).

Our method consists of two main steps: *identifying regular and irregular maps*; and *clustering regular maps*. Fig. 10 summarizes the methodology.

A. Identifying Regular and Irregular Maps

Consider the data matrix

$$\mathbf{X} = \begin{bmatrix} | & | & \dots & | \\ \mathbf{x}_1 & \mathbf{x}_2 & \dots & \mathbf{x}_m \\ | & | & \dots & | \end{bmatrix} \in \mathbb{R}^{d \times m}, \quad (1)$$

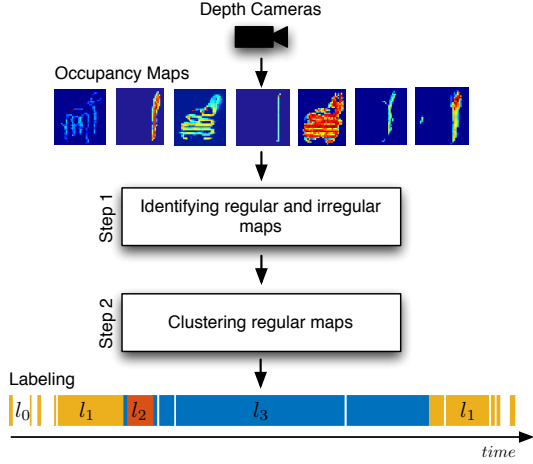


Fig. 10. Diagram summarizing the two main steps of the proposed queue classification methodology.

where column \mathbf{x}_i is a vectorized occupancy map, d is the data dimension and m is the number of maps³.

A map \mathbf{x}_i is represented by a convex combination of other maps, being modeled as

$$\mathbf{x}_i = \sum_{j=1, j \neq i}^m \mathbf{x}_j c_{ji} \quad (2)$$

$$\sum_{j=1, j \neq i}^m c_{ji} = 1, \quad c_{ji} \geq 0$$

where c_{ji} is the coefficient that relates map j with map i . Because a map should be expressed as a combination of maps belonging to the same cluster/subspace, our goal is to find the subspaces that best explain all the data. In matrix form, the model is given by

$$\mathbf{X} = \mathbf{X}\mathbf{C}, \quad (3)$$

with

$$\mathbf{1}_m^T \mathbf{C} = \mathbf{1}_m^T$$

$$\mathbf{C} \geq \mathbf{0}_{m \times m}$$

$$\text{diag}(\mathbf{C}) = \mathbf{0}$$

where $\mathbf{C} \in \mathbb{R}^{m \times m}$ is the coefficients matrix and $\mathbf{1}_m$ is a vector of ones with dimension m . Imposing the null diagonal of \mathbf{C} , $\text{diag}(\mathbf{C}) = \mathbf{0}$, excludes the trivial solution of a map explaining itself. The irregularity of a map is measured by how much the reconstruction of that map violates the linear model. This is given by

$$\mathcal{I}_i = \|\mathbf{x}_i - \mathbf{X}\mathbf{c}_i\|_1, \quad (4)$$

where the operator $\|\cdot\|_1$ is the ℓ_1 -norm and \mathbf{c}_i is the i -th column of \mathbf{C} . Our goal is to find the convex combination that best reconstructs each map, in the sense of minimizing

³Bold capital letters, \mathbf{A} , represent matrices. Bold lower-case letters, \mathbf{a} , represent column vectors. Bold lower-case letters with subscript, \mathbf{a}_i , represent the i^{th} column of matrix \mathbf{A} . Scalars are denoted by non-bold lower-case letters, a . The scalar element in row j and column i of matrix \mathbf{A} is denoted by a non-bold lower-case letter with two subscripts, a_{ji} .

the irregularity measure. Then, we wish to generate map \mathbf{x}_i with a small number of maps. By using the ℓ_1 -norm in (4), we are inducing sparsity in the error \mathcal{I}_i and consequently in \mathbf{c}_i .

The coefficients are obtained by solving the following optimization problem

$$\min_{\mathbf{C}} \mathcal{I} \quad (5)$$

$$\text{s.t. } \text{diag}(\mathbf{C}) = \mathbf{0}$$

$$\mathbf{1}_m^T \mathbf{C} = \mathbf{1}_m^T$$

$$\mathbf{C} \geq \mathbf{0}_{m \times m},$$

where

$$\mathcal{I} = \|\mathbf{X} - \mathbf{X}\mathbf{C}\|_1 \quad (6)$$

is the global irregularity measure of the data and operator $\|\cdot\|_1$ is the L_1 matrix norm. The solution is computed in parallel by solving for each \mathbf{c}_i separately [3].

By solving (5) we generate the map \mathbf{x}_i with the other maps in \mathbf{X} . However, when the error \mathcal{I}_i is too large, a map is an outlier (a unique pattern). Therefore, the irregularity \mathcal{I}_i is in fact a measure of uniqueness of the map \mathbf{x}_i within the data set. Fig. 11 shows the irregularity measure, \mathcal{I}_i , for m occupancy maps corresponding to a full day. As expected, maps with

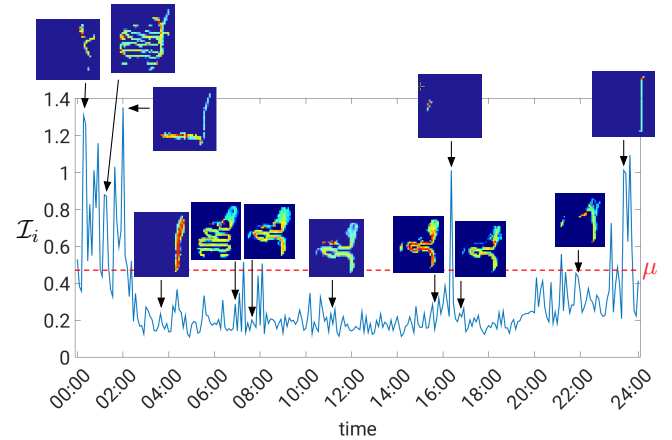


Fig. 11. Irregularity measure for a complete day. Some of the corresponding occupancy maps are presented to show that higher \mathcal{I}_i values correspond to more peculiar patterns.

lower \mathcal{I}_i are maps capturing typical states of the queue. On the other hand, large values correspond to the peculiar or occasional patterns.

We assume a maximum percentage, p , of outliers/irregular maps in the data. Thereby, we label as *irregular* the $p\%$ of maps with highest irregularity and the others as *regular*⁴. As will be clear later, the methodology is robust to a large range of p values.

Note that in [3] these irregular observations correspond to physical keypoints of a shape/model. Whereas here we interpret them as maps corresponding to unique patterns in the data.

⁴This is equivalent to apply a threshold μ to \mathcal{I}_i to divide the data into two groups [3].

B. Clustering Regular Maps

Solving (5), we are able to identify regular and irregular (outlier) patterns. Filtering out outliers, the data can be clustered using common clustering methods. Here, we take advantage of the sparse coding framework. Note that $\mathbf{C} + \mathbf{C}^T$ defines an undirected graph where the nodes represent the maps and edges represent association (non-null coefficients) between maps. Because, the number of classes K is unknown *a priori*, we estimate K by estimating the number of zero eigenvalues of the Laplacian of this graph. However, small clusters (with few points) have small impact in the eigenvalues and, when such clusters exist, K is underestimated. To retrieve the smaller clusters, we segment the data into a larger number, γ , of linear subspaces and use a measure intrinsic to the model to compute the distance between the subspaces. If this distance is small, clusters are merged.

The metric we use is the Normalized Subspace Inclusion (NSI), a distance between subspaces of any dimension [35]. Formally, it is defined as

$$NSI(\mathcal{L}_1, \mathcal{L}_2) = \frac{\text{tr}(\mathbf{U}_1^T \mathbf{U}_2 \mathbf{U}_2^T \mathbf{U}_1)}{\min(d_1, d_2)}, \quad (7)$$

where \mathcal{L}_1 and \mathcal{L}_2 are linear subspaces in \mathbb{R}^n , \mathbf{U}_1 and \mathbf{U}_2 are their orthonormal basis and d_1, d_2 are the subspaces dimensions. This metric measures inclusion of subspaces, generalizing the angle between two subspaces by considering all their principal directions.

Fig. 12 shows an affinity matrix for six clusters. For each cluster we show here only one of its maps. It is clear that the NSI value between clusters that correspond to very similar configurations is close to 1.

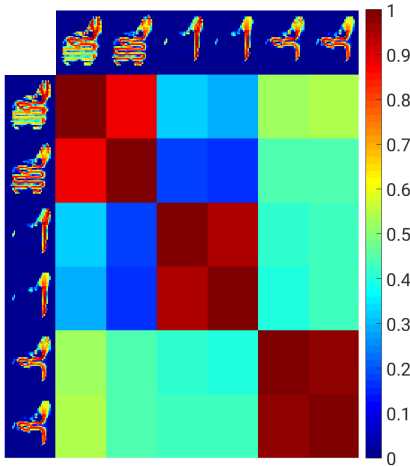


Fig. 12. NSI affinity matrix for six exemplifying clusters. For each cluster, we show a map belonging to it. Pairs of clusters corresponding to similar configuration have NSI value close to 1.

Clusters are merged if their pair-wise NSI value is above a threshold. Similarly, after this step, we reassess the maps labeled as *irregular*. We compute the pair-wise NSI affinity for each irregular map and cluster. The map is unified to the cluster with larger affinity if the value is above a threshold, otherwise, the maps remain labeled *irregular*. This consoli-

ation step, allows a large range for $p\%$ in the selection of irregular/regular patterns.

C. Methodology Summary

The methodology proposed in this section is summarized in Algorithm 1. First, we solve (5) to compute the coefficients that relate the patterns (line 1) and then we rank the maps by irregularity to identify regular and irregular maps (line 2). Next, we estimate the number of clusters and partition regular data accordingly (lines 3 and 4). Then, clusters are consolidated using the affinity measure (lines 5 and 6). Finally, irregular maps are classified according to the consolidated clusters (line 7). The output is the labeling for all data points and the corresponding partition into regular and irregular patterns.

Next, we present results of applying this methodology to real data.

Algorithm 1 Identifying and clustering regular occupancy maps in the data.

Input: \mathbf{X} - Data matrix
 p - % of maps to label as irregular
 th - NSI threshold
Output: \mathbf{X}_{reg} - Regular data
 \mathbf{X}_{irreg} - Irregular data
 cl_{reg} - Regular data class labels

Step 1: Identifying Regular and Irregular Maps

- 1: $\mathcal{I} \leftarrow$ Solve (5) for \mathbf{C}
- 2: $\mathbf{X}_{reg}, \mathbf{X}_{irreg} \leftarrow$ Divide regular and irregular data according to p and \mathcal{I}

Step 2: Clustering Regular Maps

- 3: $\gamma \leftarrow$ Estimate number of clusters
 - 4: $cl_{reg} \leftarrow$ Segment \mathbf{X}_{reg} into γ clusters
 - 5: $affinity \leftarrow$ Compute NSI between γ clusters
 - 6: $cl_{NSI} \leftarrow$ Merge clusters in cl_{reg} with affinity $> th_{NSI}$
 - 7: $cl_{reg}, \mathbf{X}_{reg}, \mathbf{X}_{irreg} \leftarrow$ Reclassify \mathbf{X}_{irreg} according to cl_{NSI}
-

VI. EXPERIMENTAL RESULTS

In this section, we present results for data sequences of one day, fourteen days and four days during Christmas time. We used seven depth cameras to cover the X-ray queue area at the Lisbon international airport. The descriptor used integrates $5min$ occupancy.

A. Analyzing One Day

Here we present in detail the results of each step of our methodology applied to one day.

Fig. 13a shows the \mathbf{C} matrix obtained by solving (5) for this day. The block diagonal shape of \mathbf{C} suggests that classes appear in sequence and do not change often during the day.

Fig. 11 shows the *irregularity* for this sequence of maps, given this matrix \mathbf{C} . After ranking the maps, we remove the

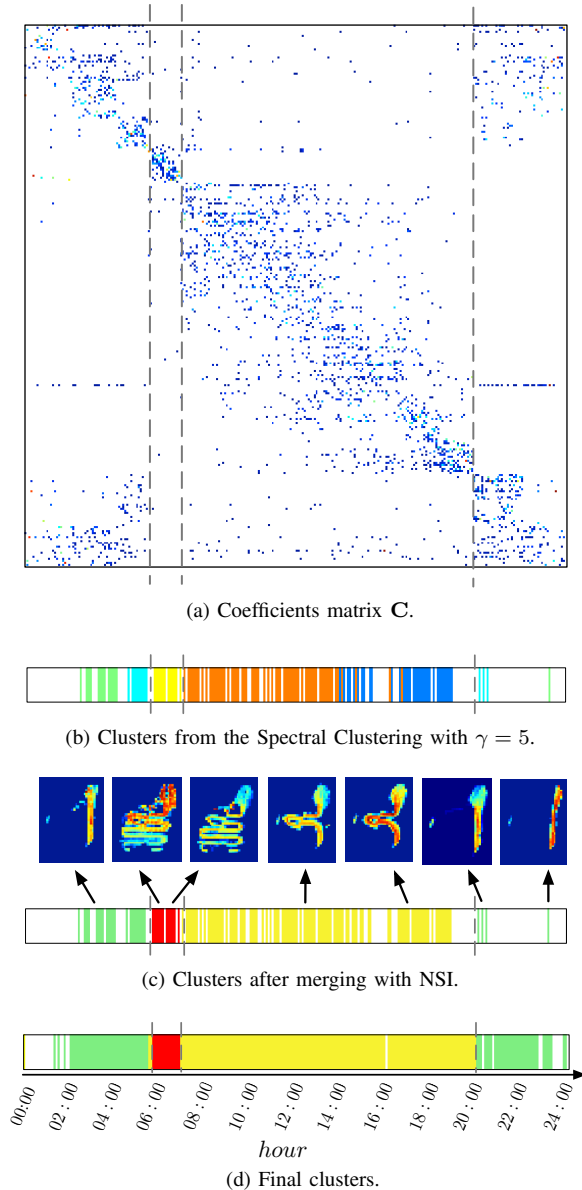


Fig. 13. Results for one day of data: (a) coefficients matrix \mathbf{C} ; (b) over-segmentation after labeling 50% of the maps as irregular; result for $\gamma = 5$, with one color per cluster (white are maps labeled as irregular); (c) consolidated clusters obtained using the NSI metric, with one color per cluster, and some of the corresponding regular maps; (d) final clusters, obtained after classifying maps initially labeled as irregular. The gray vertical dashed line in all sub-figures allows to relate coefficients in \mathbf{C} with clustering results.

50% with highest irregularity. Next, we partition the *regular* data (50% with lowest error) in 5 clusters using spectral clustering⁵. Fig. 13b shows the obtained labels, with one color per cluster and irregular maps in white. By consolidating over-segmented clusters with the NSI metric, we obtained three clusters (green, yellow and red labels) corresponding to three different queue configurations, depicted in Fig. 13c. Finally, we classified the 50% maps previously labeled as irregular to assess if they belong to any regular clusters. This results in the final classification of Fig. 13d, where 11% of the maps remain labeled *irregular*.

⁵The adjacency matrix for the Spectral Clustering is $\mathbf{C} + \mathbf{C}^T$.

During the periods 00:00am - 06:15am and 07:45pm - 11:59pm, the queue had low inflow of passengers and people would go straight from the entrance to the exit of the queue (corresponding to green label in Fig. 13d). The period with largest passenger inflow occurs between 06:15am and 07:15am (shown with red label). In this period, the queue structure is more complex, occupying a larger area to accommodate all passengers. Yellow label corresponds to a configuration with moderate flow. Irregular maps, with white label, occur mainly in the night periods (with low passenger inflow), when cleaning and maintenance operations are performed.

B. Analyzing an Extended Time Period

Fig. 14 shows results for 14 days of operation. The color labeling is shown for each day separately, although we applied the methodology to all data, with $\mathbf{X} \in \mathbb{R}^{d \times 3583}$. These colors correspond to the same configurations of Fig. 13. White label is associated with irregular or empty maps⁶.

Although all days are different from each other, periods with more inflow look similar: between 06:00am and 07:00am or between 06:00pm and 07:00pm. Irregular periods of time, as the ones depicted in Fig. 15, occur mainly in the early or late hours of the day and represent 12% of the fourteen days, a time lapse of around 39 hours⁷. Without identifying the outliers, the clusters computed by common approaches are contaminated and the corresponding subspaces may not represent the meaningful classes.

Although in these fourteen days only three clusters are identified, other time periods include different patterns. Fig. 16 shows four days during Christmas, from December 23 to 26. Traditionally, the number of departing passengers decreases during Christmas at the Lisbon international airport. Business trips decrease and the majority of the inflow is in the arrivals. During this period, a new cluster appears. This cluster, labeled with blue, is different from the three previously analyzed and is formed by maps corresponding to staff walking in a completely different pattern near the queue, during periods without passengers. This (small) class was unknown and different from the ones previously identified, however, our methodology managed to identify it.

As we previously showed in Fig. 8, similar passenger count at specific periods corresponds to different queue patterns. Fig. 17 shows the same occurs for full days. This is due to several factors affecting the state of the queue, such as the number of open X-ray gates, number of staff members operating or luggage contents, for example. In other words, for the same number of passengers, the service can be operated differently. This can be caused by several factors, such as the number of service lanes, different operational teams, number of staff members or queue guides incorrectly placed (we did not have access to data to assess what caused the different functioning state).

⁶Empty maps were not included in the data matrix.

⁷Day 3 has a large period of time without labeling because the acquisition system was off.

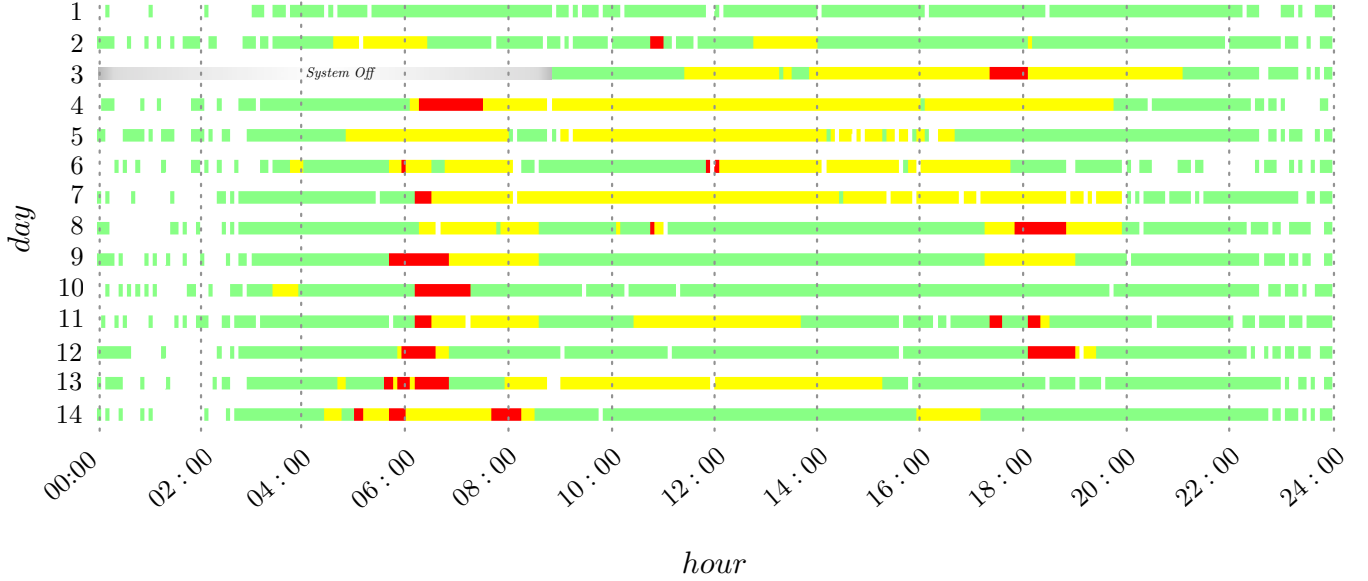


Fig. 14. Results of our methodology for 14 days of data, with $\mathbf{X} \in \mathbb{R}^{d \times 3583}$. Days are shown separately for easier analysis. Each queue configuration is labeled with a different color, with white corresponding to irregular periods. Day 3 has a large period without labeling, identified in gray, because the acquisition system was off.

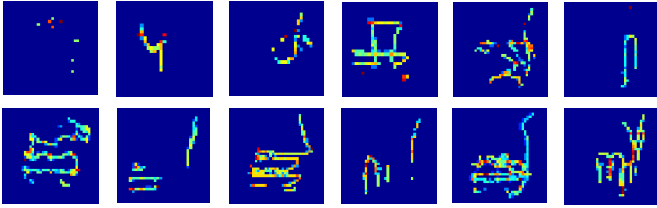


Fig. 15. Some of the irregular maps identified within a 14 day period.

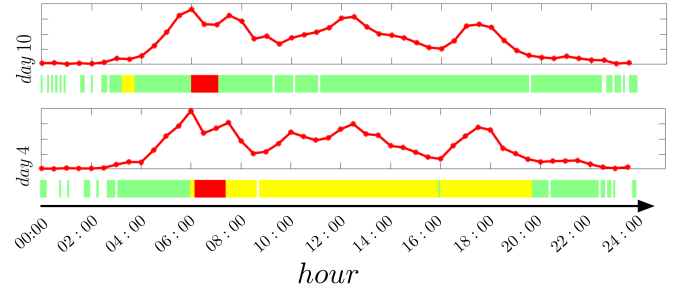


Fig. 17. Counting and labeling for two different days. Although the counting is similar, the days are different.

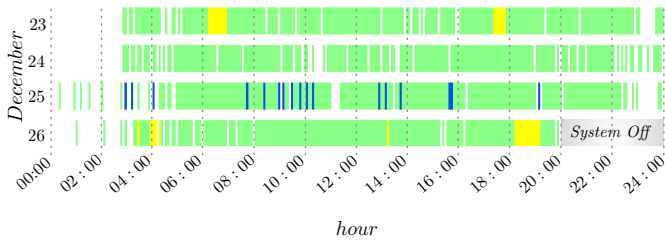


Fig. 16. Queue configuration clusters at Christmas time. Due to the decreasing number of passengers as Christmas day approaches, the inflow decreases and a new cluster appears, shown in blue. This cluster corresponds to maps with staff passing by near the empty queue.

VII. DISCUSSION

We propose an unsupervised approach with few parameters to setup.

The first parameter is the period of time covered by each occupancy map, *e.g.*, $30s, 1min, 5min$. This period of time should be chosen depending on the activity we want to capture with the descriptor. For these experiments, we empirically chose $5min$ maps, that showed to be a good trade-off between computational cost and data filtering.

Another parameter is the period of time in which we search for clusters. In this paper, we use one day, four days and

two weeks but we can choose shorter or longer periods. Our methodology presents consistent results and similar clusters can be identified whether analyzing a day by itself or combined with other days, including smaller clusters.

Fig. 18 shows the affinity matrix for nine clusters in a period where one of the (seven) cameras broke. For each cluster, we show the mean of its maps. Clusters 7, 8 and 9 are similar except in the area where the camera failed, in the middle left side of 9. Similarly, cluster 6 corresponds to the same queue state as clusters 4 and 5. Our method degrades gracefully in the presence of perturbations and clusters 6 and 9 have high affinity with the corresponding configuration classes.

Although the methodology presented in this paper is unsupervised, when working with real data and operational scenarios, interaction with end users/experts is very useful. Because of the large amount of data, airport experts are not able to describe classes *a priori*. By providing only representative patterns, our methodology works as a filter and saves users from the overwhelming load of interpreting all data. When presented with the relevant patterns, the airport experts recognize the classes as meaningful and understand

the affinity matrix. This allows them to empirically define semantics to design a classifier customized to their needs. Finally, with these classes, and applying queuing and discrete events theory, we are able to compute individual and more accurate models for each state.

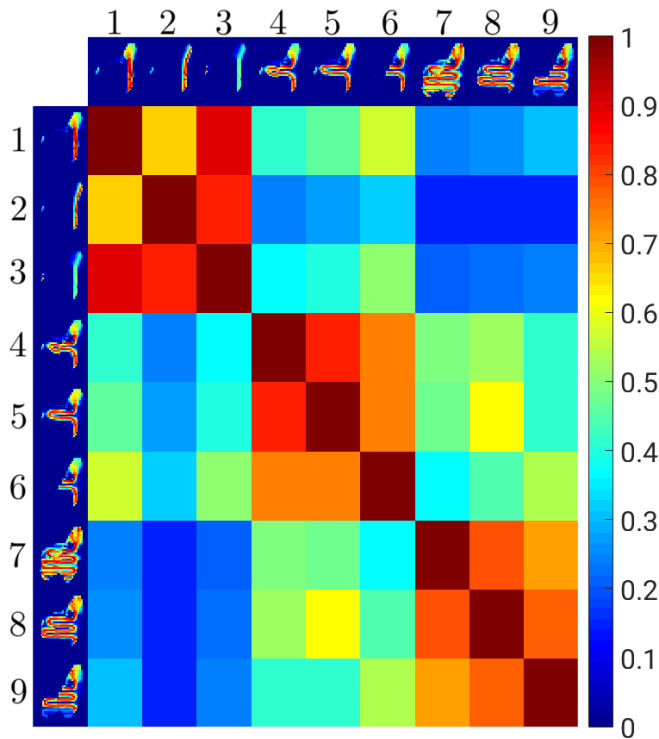


Fig. 18. NSI affinity matrix including maps with missing data. The characteristics of the descriptor and NSI allow for a smooth degradation of the affinity value when missing data.

VIII. CONCLUSION

We proposed a new descriptor to characterize the flow of people in large public infrastructures. Based on 3D data and without tracking people, we provided an occupancy map of the space—a very useful indicator of the service performance. We proposed an unsupervised methodology to identify and cluster these occupancy maps, without knowing their number or shape/configuration *a priori*. The approach is divided into two main steps: identify regular and irregular periods/maps, and cluster the regular maps into classes corresponding to the different queue configurations. This methodology proposes a continuous irregularity measure for each map. The first step of the approach uses this measure as a means to identify the most abnormal maps in the data set. The second step segments the regular maps, based on an estimate of the number of clusters, and then consolidates the clusters using the Normalized Subspace Inclusion (NSI) metric.

The approach gave consistent results, independently of the quantity of data analyzed, with the descriptor and NSI having smooth deterioration in the presence of missing data.

Despite including different days, they present similar patterns: the busiest hours occur in the same periods of the day. Finally, irregular maps exist mainly during late night, when maintenance operations are due.

As future work, we plan to augment the model to account for more information sources, *e.g.*, velocity, flight schedule, flight destiny, in order to strengthen the assessment of the service performance.

ACKNOWLEDGMENTS

This work was done in institutional collaboration with Thales Portugal S.A. and ANA *Aerportos de Portugal*, within the SMART-er project. The authors would like to specially thank João Mira (Thales), Francisco Oliveira and Isabel Rebelo (ANA).

REFERENCES

- [1] S. Denman, T. Kleinschmidt, D. Ryan, P. Barnes, S. Sridharan, and C. Fookes, "Automatic surveillance in transportation hubs: No longer just about catching the bad guy," *Expert Systems with Applications*, vol. 42, no. 24, pp. 9449–9467, 2015.
- [2] R. Felkel and D. Klann, "Comprehensive passenger flow management at frankfurt airport," *Journal of Airport Management*, vol. 6, no. 2, pp. 107–124, 2012.
- [3] J. Vongkulbhisal, R. Cabral, J. Costeira, and F. de la Torre, "Motion from structure (mfs): Searching for 3d objects in cluttered point trajectories," in *CVPR 2016*, 2016.
- [4] M. Soltanolkotabi and E. J. Candes, "A geometric analysis of subspace clustering with outliers," *The Annals of Statistics*, pp. 2195–2238, 2012.
- [5] E. Elhamifar and R. Vidal, "Sparse subspace clustering: Algorithm, theory, and applications," *Pattern Analysis and Machine Intelligence, IEEE Transactions on*, vol. 35, no. 11, pp. 2765–2781, 2013.
- [6] W. Chen, F. Guo, and F.-Y. Wang, "A survey of traffic data visualization," *IEEE Transactions on Intelligent Transportation Systems*, vol. 16, no. 6, pp. 2970–2984, 2015.
- [7] P. P.-Y. Wu and K. Mengersen, "A review of models and model usage scenarios for an airport complex system," *Transportation Research Part A: Policy and Practice*, vol. 47, pp. 124–140, 2013.
- [8] G. Guizzi, T. Murino, and E. Romano, "A discrete event simulation to model passenger flow in the airport terminal," *Mathematical Methods and Applied Computing*, vol. 2, pp. 427–434, 2009.
- [9] S. L. Dorton and D. Liu, "Effects of baggage volume and alarm rate on airport security screening checkpoint efficiency using queuing networks and discrete event simulation," *Human Factors and Ergonomics in Manufacturing & Service Industries*, vol. 26, no. 1, pp. 95–109, 2016.
- [10] R. R. Gilliam, "An application of queuing theory to airport passenger security screening," *Interfaces*, vol. 9, no. 4, pp. 117–123, 1979.
- [11] S. Takakuwa and T. Oyama, "Modeling people flow: simulation analysis of international-departure passenger flows in an airport terminal," in *Proceedings of the 35th conference on Winter simulation: driving innovation*. Winter Simulation Conference, 2003, pp. 1627–1634.
- [12] R. De Lange, I. Samoilovich, and B. van der Rhee, "Virtual queuing at airport security lanes," *European Journal of Operational Research*, vol. 225, no. 1, pp. 153–165, 2013.
- [13] C. Gao, J. Liu, Q. Feng, and J. Lv, "People-flow counting in complex environments by combining depth and color information," *Multimedia Tools and Applications*, pp. 1–17, 2016.
- [14] L. Del Pizzo, P. Foggia, A. Greco, G. Percannella, and M. Vento, "A versatile and effective method for counting people on either rgb or depth overhead cameras," in *Multimedia & Expo Workshops (ICMEW), 2015 IEEE International Conference on*. IEEE, 2015, pp. 1–6.
- [15] H. Fu, H. Ma, and H. Xiao, "Scene-adaptive accurate and fast vertical crowd counting via joint using depth and color information," *Multimedia Tools and Applications*, vol. 73, no. 1, pp. 273–289, 2014.
- [16] A. Albiol and J. Silla, "Statistical video analysis for crowds counting," in *Image Processing (ICIP), 2009 16th IEEE International Conference on*. IEEE, 2009, pp. 2569–2572.
- [17] J. Barandiaran, B. Murguia, and F. Boto, "Real-time people counting using multiple lines," in *Image Analysis for Multimedia Interactive Services, 2008. WIAMIS'08. Ninth International Workshop on*. IEEE, 2008, pp. 159–162.
- [18] Z. Zhao, H. Li, R. Zhao, and X. Wang, "Crossing-line crowd counting with two-phase deep neural networks," in *European Conference on Computer Vision*. Springer, 2016, pp. 712–726.

- [19] C. Zhang, H. Li, X. Wang, and X. Yang, "Cross-scene crowd counting via deep convolutional neural networks," in *Proceedings of the IEEE Conference on Computer Vision and Pattern Recognition*, 2015, pp. 833–841.
- [20] Y. Zhang, D. Zhou, S. Chen, S. Gao, and Y. Ma, "Single-image crowd counting via multi-column convolutional neural network," in *Proceedings of the IEEE Conference on Computer Vision and Pattern Recognition*, 2016, pp. 589–597.
- [21] Z. Ma and A. Chan, "Crossing the line: Crowd counting by integer programming with local features," in *Proceedings of the IEEE Conference on Computer Vision and Pattern Recognition*, 2013, pp. 2539–2546.
- [22] S. Mukherjee, S. Gil, and N. Ray, "Unique people count from monocular videos," *The Visual Computer*, vol. 31, no. 10, pp. 1405–1417, 2015.
- [23] H. Nallaivarothayan, C. Fookes, S. Denman, and S. Sridharan, "An mrf based abnormal event detection approach using motion and appearance features," in *Advanced Video and Signal Based Surveillance (AVSS), 2014 11th IEEE International Conference on*. IEEE, 2014, pp. 343–348.
- [24] X. Wang, X. Ma, and W. E. L. Grimson, "Unsupervised activity perception in crowded and complicated scenes using hierarchical bayesian models," *Pattern Analysis and Machine Intelligence, IEEE Transactions on*, vol. 31, no. 3, pp. 539–555, 2009.
- [25] M. Roshtkhari and M. Levine, "Online dominant and anomalous behavior detection in videos," in *Proceedings of the IEEE Conference on Computer Vision and Pattern Recognition*, 2013, pp. 2611–2618.
- [26] A. M. Cheriyyadat and R. J. Radke, "Detecting dominant motions in dense crowds," *IEEE Journal of Selected Topics in Signal Processing*, vol. 2, no. 4, pp. 568–581, 2008.
- [27] J. Lei, T. Jiang, K. Wu, H. Du, G. Zhu, and Z. Wang, "Robust k-means algorithm with automatically splitting and merging clusters and its applications for surveillance data," *Multimedia Tools and Applications*, pp. 1–17, 2016.
- [28] M. M. Kalayeh, S. Mussmann, A. Petrakova, N. d. V. Lobo, and M. Shah, "Understanding trajectory behavior: A motion pattern approach," *arXiv preprint arXiv:1501.00614*, 2015.
- [29] B. T. Morris and M. M. Trivedi, "Learning, modeling, and classification of vehicle track patterns from live video," *IEEE Transactions on Intelligent Transportation Systems*, vol. 9, no. 3, pp. 425–437, 2008.
- [30] T. W. Liao, "Clustering of time series data—a survey," *Pattern recognition*, vol. 38, no. 11, pp. 1857–1874, 2005.
- [31] Z. Hou and X. Li, "Repeatability and similarity of freeway traffic flow and long-term prediction under big data," *IEEE Transactions on Intelligent Transportation Systems*, vol. 17, no. 6, pp. 1786–1796, 2016.
- [32] Z. Wu and R. J. Radke, "Real-time airport security checkpoint surveillance using a camera network," in *Computer Vision and Pattern Recognition Workshops (CVPRW), 2011 IEEE Computer Society Conference on*. IEEE, 2011, pp. 25–32.
- [33] J. Candamo, M. Shreve, D. B. Goldgof, D. B. Sapper, and R. Kasturi, "Understanding transit scenes: A survey on human behavior-recognition algorithms," *IEEE Transactions on Intelligent Transportation Systems*, vol. 11, no. 1, pp. 206–224, 2010.
- [34] J. Carvalho, M. Marques, J. P. Costeira, and P. M. Jorge, "Detecting people in large crowded spaces using 3d data from multiple cameras," in *Proceedings of the 11th Joint Conference on Computer Vision, Imaging and Computer Graphics Theory and Applications*, 2016, pp. 218–225.
- [35] N. P. d. Silva and J. P. Costeira, "The normalized subspace inclusion: Robust clustering of motion subspaces," in *Computer Vision, 2009 IEEE 12th International Conference on*. IEEE, 2009, pp. 1444–1450.